HHS Public Access

Author manuscript

J Am Chem Soc. Author manuscript; available in PMC 2020 June 26.

Published in final edited form as:

J Am Chem Soc. 2019 June 26; 141(25): 9753–9757. doi:10.1021/jacs.9b00651.

Supramolecular Assembly of High-Density Lipoprotein Mimetic Nanoparticles Using Lipid-Conjugated Core Scaffolds

Stephen E. Henrich[#], **Bong Jin Hong**[⊥], **Jonathan S. Rink**[#], **SonBinh T. Nguyen**[*,⊥,§,†], **C. Shad Thaxton**[*,#,§,†,‡]

[#]Department of Urology, Feinberg School of Medicine, Northwestern University, 303 E. Chicago Avenue, Chicago, Illinois 60611, United States

[‡]Simpson Querrey Institute for BioNanotechnology, Northwestern University, 303 E. Chicago Avenue, Chicago, Illinois 60611, United States

[†]Robert H. Lurie Comprehensive Cancer Center, Northwestern University, 303 E. Chicago Avenue, Chicago, Illinois 60611, United States

[⊥]Department of Chemistry, Northwestern University, 2145 Sheridan Road, Evanston, Illinois 60208, United States

[§]International Institute for Nanotechnology, Northwestern University, 2145 Sheridan Road, Evanston, Illinois 60208, United States

Abstract

Synthetic high-density lipoprotein (HDL) mimics have emerged as promising therapeutic agents. However, approaches to date have been unable to reproduce key features of spherical HDLs, which are the most abundant human HDL species. Here, we report the synthesis and characterization of spherical HDL mimics using lipid-conjugated organic core scaffolds. The core design motif constrains and orients phospholipid geometry to facilitate the assembly of soft-core nanoparticles that are approximately 10 nm in diameter and resemble human HDLs in their size, shape, surface chemistry, composition, and protein secondary structure. These particles execute salient HDL functions, including efflux of cholesterol from macrophages, cholesterol delivery to hepatocytes, support lecithin:cholesterol acyltransferase activity, and suppress inflammation. These results represent a significant step toward a genuine functional mimic of human HDLs.

High-density lipoproteins (HDL) are dynamic nanoparticles that circulate in the blood and transport cholesterol. Clinically, elevated HDL cholesterol levels are associated with reduced risk of atherosclerotic cardiovascular disease (ASCVD).[1,2] At the cellular level, HDLs target macrophages and hepatocytes to remove and deliver cholesterol respectively [a process known as reverse cholesterol transport (RCT)], which leads to reduced inflammation and

[*]**Corresponding Authors:** cthaxton003@northwestern.edu, stn@northwestern.edu.

ASSOCIATED CONTENT

Supporting Information

The Supporting Information is available free of charge on the ACS Publications website at DOI: 10.1021/jacs.9b00651.

Detailed information regarding materials, methods, and supplementary results (PDF)

The authors declare no competing financial interest.

atherosclerotic burden.[3,4] Due to the beneficial association between HDL and ASCVD, the cell-specific targeting properties of HDL, and the intrigue of using HDLs for targeted drug delivery, tremendous effort has focused on synthesizing HDLs that resemble their natural counterparts.[5]

There are multiple HDL species in the blood that serve as synthetic targets. Immature HDLs are cholesterol-poor and discoidal in shape, consisting mainly of the HDL-defining protein, apolipoprotein A-I (apoA-I), and phospholipids. Mature forms of HDL, which also harbor apoA-I and a surface layer of phospholipids, are rich in cholesterol and cholesteryl esters, and are roughly spherical (Figure 1). Spherical HDLs comprise the majority of HDLs in circulation.[6,7] Yet, synthetic forms of HDL used in the clinic have exclusively resembled immature, discoidal HDL, largely because these recombinant HDLs (rHDL) are relatively easy to fabricate by self-assembling phospholipids and apoA-I.[8–12] Clinical trials using rHDLs have shown some promise, but also reveal that there is significant room for improvement.[10–12] There remains ongoing debate regarding the relative antiatherosclerotic functions of discoidal and spherical HDLs, and hence a question about which subspecies should be mimicked by bioinspired therapeutics. The prevailing view has been that discoidal HDLs are responsible for the majority of RCT activity and ASCVD risk reduction.[13] However, larger, spherical HDL species have specifically been shown to be associated with reduced ASCVD risk.[14,15] This correlative data, in combination with recent metabolic evidence,[16] has led some investigators to propose an alternative model[17] that suggests spherical HDLs play a prominent role in atheroprotection. To this end, we sought to develop a spherical HDL mimic to both address the dearth of synthetic, spherical HDLs in the literature, and provide a tool for interrogating the therapeutic functions of discoidal and spherical HDLs.

Spherical HDLs are challenging to synthesize due to the enzymatic steps required to mature discoidal HDLs into cholesterol- and cholesteryl ester-containing spherical HDLs. Our group, and others, have attempted to circumvent these biological maturation steps by using inorganic nanoparticles as templates.[18–20] The templates can be functionalized with phospholipids and apoA-I, and successfully restrict the size of HDL mimics to < 15 nm in diameter.[21] These HDL-like nanoparticles have demonstrated exquisite properties for modulating cellular cholesterol,[22,23] *in vivo* imaging,[24] and drug delivery.[25] However, these materials fail to recapitulate a critical feature of native HDLs, namely a robust, soft material core capable of dynamically loading and off-loading cholesterol and cholesteryl esters. We note that many other HDL-like platforms have been reported, including soft-core, discoidal particles using amphiphilic peptides,[26] rationally engineered HDL-like nanodiscs,[27,28] and drug-loaded rHDLs.[29–31]

Herein, we describe the synthesis of spherical HDL-like nanoparticles using lipid-conjugated core scaffolds. Three organic scaffolds varying in size and composition were investigated. The first scaffold is a highly hydrophobic small molecule-phospholipid conjugate (PL_4) that was synthesized using copper-free click chemistry. Specifically, a headgroup-modified phospholipid harboring a ring-strained alkyne, 1,2-dipalmitoyl-*sn*-glycero-3-phosphoethanolamine-*N*-dibenzocy-clooctyl (DBCO PL), was click-coupled to *tetrakis*(4-azidophenyl)methane, a small molecule with four terminal azides ($SM\text{-}Az_4$)

(Figure 2a; SI, Figure S6) to yield PL_4. The second (9-DNA-PL_4) and third (18-DNA-PL_4) core scaffolds are amphiphilic DNA-linked PL_4 cores (Figure 2b) with different DNA linker length (9- vs 18-mer dsDNA). While DNA linkers enhance the solubility of the cores in aqueous solution, externally oriented phospholipid tails enable hydrophobic interaction with apoA-I and phospholipids. The arm lengths of these core scaffolds can be easily tuned by adjusting the length of DNA linkers. Both DNA-PL_4 cores were synthesized in a two-step sequence (SI, Section S2a). First, we synthesized DNA-phospholipid conjugates (ssDNA-PL), and tetrahedral small molecule-DNA hybrids ($SMDH_4$). Second, ssDNA-PL and $SMDH_4$ with complementary base-pairing sequences were hybridized to yield the final DNA-PL_4 cores (Figure 2b; SI, Figures S1–4, Table S1).

Using the resulting core scaffolds, we carried out the assembly of lipid conjugate HDL-like nanoparticles (LC HDL NPs). We first prepared liposomes from 1,2-dipalmitoyl-*sn*-glycero-3-phosphocholine (DPPC) (SI, Section 2c). PL_4 scaffolds were then prepared as thin films, while DNA-PL_4 scaffolds were prepared in aqueous buffer. ApoA-I protein and DPPC liposomes were added to the core scaffolds and the mixture was subjected to three rounds of sonication, allowed to relax on ice, then filtered and concentrated using a 50 kDa MWCO spin column (Figure 2c). Schematic models of LC HDL NPs, gold nanoparticle-templated HDL NPs (Au HDL NPs), and human HDLs are shown in Figure 2d.

Transmission electron microscopy (TEM) imaging revealed a relatively monodisperse population of nanoparticles for the assemblies using PL_4 and 9-DNA-PL_4 scaffolds (TEM diameter = 10 ± 2 nm and 9 ± 2 nm, respectively) (Figure 2g; SI, Figure S8). Notably, the morphology of these particles was not characteristic of immature, discoidal HDLs, or rHDLs, both of which exhibit a hallmark rouleaux formation of stacked phospholipid discs.[21,26,32] Instead, the particles appeared roughly spherical, with a peripheral hypodense region. Dynamic light scattering experiments revealed hydrodynamic diameters resembling those of human HDLs (D_H = 13.8 ± 3.9 and 13.3 ± 4.6 nm for PL_4 HDL NPs and 9-DNA-PL_4 HDL NPs, respectively) (SI, Table S2). Size-exclusion chromatography (SEC) demonstrated peak retention volumes of 8.22 and 8.58–8.88 mL for 9-DNA-PL_4 HDL NPs and PL_4 HDL NPs, respectively (SI, Figure S14; see also Section S11f2 for additional discussions). SEC traces of LC HDL NPs also revealed right-sided tails consistent with a small amount of free apoA-I (10.13 mL retention volume), which was also observed in human HDL controls (see SI, Section 11d for discussion).

While assemblies using PL_4 and 9-DNA-PL_4 scaffolds successfully generated sub-20 nm particles, the assemblies using 18-DNA-PL_4 scaffolds persisted as large vesicular structures after the addition of DPPC and apoA-I (SI, Figure S9). We hypothesize that this is a result of the hybrid's size being prohibitively large for apoA-I assembly. Interestingly, 9-DNA-PL_4 HDL NPs were not significantly larger than PL_4 HDL NPs. This result, in conjunction with the lack of assembly using 18-DNA-PL_4, suggests that LC HDL NP size may be determined primarily by apoA-I protein folding, irrespective of core size below a certain threshold. For convenience henceforth, we refer to the particles formed using 9-DNA-PL_4 scaffolds simply as DNA-PL_4 HDL NPs.

To characterize particle structure in terms of apoA-I protein conformation, circular dichroism measurements were carried out on LC HDL NPs and controls, and analyzed using three distinct reference protein databases. PL_4 HDL NPs and DNA-PL_4 HDL NPs were found to closely resemble human HDLs in secondary structure, while Au HDL NPs exhibited excess α helicity and less β sheet and turn content (Table 1 and Figure 2f). To characterize LC HDL NP structure further, we investigated the apoA-I oligomerization state by crosslinking LC HDL NPs with bis(sulfosuccinimidyl)suberate followed by immunoblot.[22] ApoA-I interaction with LC cores was found to induce stable oligomer formation (SI, Figure S13). Notably, the surface zeta potentials of LC HDL NPs were more negative ($\zeta = -21 \pm 2$ mV for PL_4 and -19 ± 1 mV for DNA-PL_4) than those for apoA-I alone ($\zeta = -10 \pm 3$ mV) or an [apoA-I + DPPC] mixture ($\zeta = -12 \pm 2$ mV), but quite similar to human HDL_2 ($\zeta = -19 \pm 2$ mV) and HDL_3 ($\zeta = -21 \pm 5$ mV). Finally, we found that the composition of LC HDL NPs closely mirrors that of HDL_2 and HDL_3, with the exception that LC HDL NPs do not contain cholesterol or cholesteryl esters (Figure 2e; see SI, Section S11e,f for molar composition data (Table S4) and additional discussions).

Complementary biological assays were carried out to investigate whether LC HDL NPs could recapitulate salient HDL functions. A critical property for HDL mimicry is the ability to efflux cholesterol from lipid-laden macrophages, which we evaluated using an *in vitro* radiolabeled cholesterol efflux assay (SI, Section S7a).[33] Briefly, J774 macrophages were loaded with tritium-labeled cholesterol ([^{3}H]-chol), cultured with cAMP to upregulate cholesterol efflux receptors, and treated with nanoparticles or controls for 4 h. The media supernatant was subjected to liquid scintillation counting to quantify percent effluxed [^{3}H]-chol, revealing that both PL_4 HDL NPs and DNA-PL_4 HDL NPs facilitated robust cholesterol efflux (PL_4: 6.2 ± 0.7%, DNA-PL_4: 6.5 ± 0.2%; 100 nM protein) in a dose-dependent manner (Figure 3a).

Encouraged by the aforementioned results, we then designed an experiment to simulate the entire RCT process in a single assay. We accomplished this by carrying out the standard radiolabel efflux assay followed by an influx step where conditioned efflux media was introduced to cultured hepatocytes (HepG2) and influx was allowed to proceed for an additional 4 h. Liquid scintillation counting analyses of all three fractions from macrophages, hepatocytes, and media supernatant revealed that LC HDL NPs exhibited superior cholesterol transport capacity compared to human HDLs, apoA-I, and Au HDL NP (Figure 3b,c). This assay demonstrates not only that LC HDL NPs are capable of robust cholesterol efflux and delivery, but also that a single-particle cohort can execute these functions sequentially by on- and off-loading cholesterol in a dynamic fashion.

Next, we investigated the efficacy of LC HDL NPs as cholesterol delivery agents independently of efflux, a function carried out in the native setting by mature HDLs. HepG2 cells were cotreated with fluorescent cholesterol (NBD-chol) and LC HDL NPs or controls, and subsequently processed for flow cytometry or confocal microscopy. Strikingly, LC HDL NPs facilitated efficient delivery of NBD-chol in only 30 min (Figure 4), with 23% of PL_4 HDL NP-treated cells being NBD-positive compared to 8.5%, 6.8%, and 5.7% for HDL_2, apoA-I, and Au HDL NP, respectively.

Native HDLs also support the enzymatic esterification of free cholesterol, a reaction carried out in the blood by the enzyme lecithin:cholesterol acyltransferase (LCAT). We found that both PL_4 and DNA-PL_4 HDL NPs supported LCAT-mediated esterification (Figure 5a). However, PL_4 HDL NPs supported substantially more esterification than DNA-PL_4 HDL NPs and Au HDL NPs, converting 87% of bound cholesterol to cholesteryl esters. This is likely due to the increased hydrophobicity of the PL_4 core, which enables efficient sequestration of cholesteryl esters.

Finally, inflammation promoted by macrophage NF-κB activity is a hallmark of ASCVD that drives disease progression and increases morbidity and mortality. To this end, we treated human monocyte NF-κB reporter cells (THP1-Dual) with lipopolysaccharide to stimulate NF-κB activity prior to treatment with LC HDL NPs or controls. While apoA-I alone exhibited no capacity to reduce NF-κB activity under these low-dosing conditions, both PL_4 HDL NPs and DNA-PL_4 HDL NPs favorably reduced NF-κB activity in a dose dependent manner, by 31% and 16% respectively at concentrations of 150 nM (Figure 5b).

In summary, we report the synthesis of soft-core, HDL-like nanoparticles with the size, shape, surface chemistry, composition, protein structure, and cholesterol transport properties that are consistent with mature human HDLs. LC HDL NPs target relevant cell types to remove and deliver cellular cholesterol and reduce inflammation, closely mimicking the salient functions of human HDLs. Because synthesis of LC HDL NPs is straightforward and does not require time-intensive and costly enzymatic maturation steps, we anticipate these nanoparticles will be strong candidates for the next generation of HDL-based therapeutics.

Supplementary Material

Refer to Web version on PubMed Central for supplementary material.

ACKNOWLEDGMENTS

This work is supported by the NIH (AG062999-01). S.E.H. gratefully acknowledges support from the NIH for an individual graduate fellowship (CA225133-02). B.J.H. and S.T.N. acknowledge support from the NIH [C54CA151880, and Core Grant P30CA060553 to the Lurie Cancer Center of Northwestern University (NU)]. C.S.T. is grateful for financial support from the NTU-NU Institute for Nanomedicine and from the CRN Regenerative Nanomedicine Catalyst Award Program at Northwestern University and the Simpson Querrey Institute for BioNanotechnology. The authors thank the Center for Advanced Microscopy at Northwestern University for their support with TEM and confocal imaging, Dr. Arsen Gaisin for assistance with SEC, and Mr. Mark Seniw for assistance in the preparation of graphic illustrations.

REFERENCES

(1). Roth GA; Huffman MD; Moran AE; Feigin V; Mensah GA; Naghavi M; Murray CJ Global and regional patterns in cardiovascular mortality from 1990 to 2013. Circulation 2015, 132, 1667–1678. [PubMed: 26503749]

(2). Shepard D; VanderZanden A; Moran A; Naghavi M; Murray C; Roth G Ischemic heart disease worldwide, 1990 to 2013: Estimates from the global burden of disease study 2013. Circ. Cardiovasc. Qual. Outcomes 2015, 8 (4), 455–456. [PubMed: 26152681]

(3). Feig JE; Rong JX; Shamir R; Sanson M; Vengrenyuk Y; Liu J; Rayner K; Moore K; Garabedian M; Fisher EA HDL promotes rapid atherosclerosis regression in mice and alters inflammatory properties of plaque monocyte-derived cells. Proc. Natl. Acad. Sci. U. S. A 2011, 108, 7166–7171. [PubMed: 21482781]

(4). Yvan-Charvet L; Wang N; Tall AR Role of HDL, ABCA1, and ABCG1 transporters in cholesterol efflux and immune responses. Arterioscler., Thromb., Vasc. Biol 2010, 30 (2), 139–143. [PubMed: 19797709]

(5). Lacko AG; Sabnis NA; Nagarajan B; McConathy WJ HDL as a drug and nucleic acid delivery vehicle. Front. Pharmacol 2015, 6, 247/1–6.

(6). Rosenson RS; Brewer HB Jr.; Chapman MJ; Fazio S; Hussain MM; Kontush A; Krauss RM; Otvos JD; Remaley AT; Schaefer EJ HDL measures, particle heterogeneity, proposed nomenclature, and relation to atherosclerotic cardiovascular events. Clin. Chem 2011, 57 (3), 392–410. [PubMed: 21266551]

(7). Kontush A; Chapman MJ Functionally defective high-density lipoprotein: a new therapeutic target at the crossroads of dyslipidemia, inflammation, and atherosclerosis. Pharmacol. Rev 2006, 58 (3), 342–374. [PubMed: 16968945]

(8). Simonsen JB Evaluation of reconstituted high-density lipoprotein (rHDL) as a drug delivery platform - a detailed survey of rHDL particles ranging from biophysical properties to clinical implications. Nanomedicine 2016, 12 (7), 2161–2179. [PubMed: 27237620]

(9). Cao YN; Xu L; Han YC; Wang YN; Liu G; Qi R Recombinant high-density lipoproteins and their use in cardiovascular diseases. Drug Discovery Today 2017, 22 (1), 180–185. [PubMed: 27591840]

(10). Andrews J; Janssan A; Nguyen T; Pisaniello AD; Scherer DJ; Kastelein JJ; Merkely B; Nissen SE; Ray K; Schwartz GG; Worthley SG; Keyserling C; Dasseux JL; Butters J; Girardi J; Miller R; Nicholls SJ Effect of serial infusions of reconstituted high-density lipoprotein (CER-001) on coronary atherosclerosis: rationale and design of the CARAT study. Cardiovasc. Diagn. Ther 2017, 7 (1), 45–51. [PubMed: 28164012]

(11). Kataoka Y; Andrews J; Duong M; Nguyen T; Schwarz N; Fendler J; Puri R; Butters J; Keyserling C; Paolini JF; Dasseux JL; Nicholls SJ Regression of coronary atherosclerosis with infusions of the high-density lipoprotein mimetic CER-001 in patients with more extensive plaque burden. Cardiovasc. Diagn. Ther 2017, 7 (3), 252–263. [PubMed: 28567351]

(12). Keyserling CH; Barbaras R; Benghozi R; Dasseux JL Development of CER-001: Preclinical dose selection through to phase I clinical findings. Clin. Drug Invest 2017, 37 (5), 483–491.

(13). Fielding CJ; Fielding PE Molecular physiology of reverse cholesterol transport. J. Lipid Res 1995, 36 (2), 211–228. [PubMed: 7751809]

(14). Li JJ; Zhang Y; Li S; Cui CJ; Zhu CG; Guo YL; Wu NQ; Xu RX; Liu G; Dong Q; Sun J Large HDL subfraction but not HDL-C is closely linked with risk factors, coronary severity and outcomes in a cohort of nontreated patients with stable coronary artery disease a prospective observational study. Medicine 2016, 95, No. e2600/1–7.

(15). Morgan J; Carey C; Lincoff A; Capuzzi D High-density lipoprotein subfractions and risk of coronary artery disease. Curr. Atheroscler. Rep 2004, 6 (5), 359–365. [PubMed: 15296702]

(16). Mendivil CO; Furtado J; Morton AM; Wang L; Sacks FM Novel pathways of apolipoprotein A-I metabolism in high-density lipoprotein of different sizes in humans. Arterioscler., Thromb., Vasc. Biol 2016, 36 (1), 156–165. [PubMed: 26543096]

(17). Sacks FM; Jensen MK From high-density lipoprotein cholesterol to measurements of function: prospects for the development of tests for high-density lipoprotein functionality in cardiovascular disease. Arterioscler., Thromb., Vasc. Biol 2018, 38 (3), 487–499. [PubMed: 29371248]

(18). Thaxton CS; Daniel WL; Giljohann DA; Thomas AD; Mirkin CA Templated spherical high density lipoprotein nanoparticles. J. Am. Chem. Soc 2009, 131 (4), 1384–1385. [PubMed: 19133723]

(19). Skajaa T; Cormode DP; Falk E; Mulder WJ; Fisher EA; Fayad ZA High-density lipoprotein-based contrast agents for multimodal imaging of atherosclerosis. Arterioscler., Thromb., Vasc. Biol 2010, 30 (2), 169–176. [PubMed: 19815819]

(20). Cormode DP; Skajaa T; van Schooneveld MM; Koole R; Jarzyna P; Lobatto ME; Calcagno C; Barazza A; Gordon RE; Zanzonico P; Fisher EA; Fayad ZA; Mulder WJ Nanocrystal core high-density lipoproteins: a multimodality contrast agent platform. Nano Lett 2008, 8 (11), 3715–3723. [PubMed: 18939808]

(21). Forte TM; Nordhausen RW Electron microscopy of negatively stained lipoproteins. Methods Enzymol 1986, 128, 442–457. [PubMed: 2425222]

(22). Luthi AJ; Lyssenko NN; Quach D; McMahon KM; Millar JS; Vickers KC; Rader DJ; Phillips MC; Mirkin CA; Thaxton CS Robust passive and active efflux of cellular cholesterol to a designer functional mimic of high density lipoprotein. J. Lipid Res 2015, 56 (5), 972–985. [PubMed: 25652088]

(23). Plebanek MP; Mutharasan RK; Volpert O; Matov A; Gatlin JC; Thaxton CS Nanoparticle targeting and cholesterol flux through scavenger receptor type B-1 inhibits cellular exosome uptake. Sci. Rep 2015, 5, 15724/1–14.

(24). Cormode DP; Roessl E; Thran A; Skajaa T; Gordon RE; Schlomka JP; Fuster V; Fisher EA; Mulder WJ; Proksa R; Fayad ZA Atherosclerotic plaque composition: analysis with multicolor CT and targeted gold nanoparticles. Radiology 2010, 256, 774–782. [PubMed: 20668118]

(25). McMahon KM; Mutharasan RK; Tripathy S; Veliceasa D; Bobeica M; Shumaker DK; Luthi AJ; Helfand BT; Ardehali H; Mirkin CA; Volpert O; Thaxton CS Biomimetic high density lipoprotein nanoparticles for nucleic acid delivery. Nano Lett 2011, 11, 1208–1214. [PubMed: 21319839]

(26). Zhao Y; Imura T; Leman LJ; Curtiss LK; Maryanoff BE; Ghadiri MR Mimicry of high-density lipoprotein: functional peptide-lipid nanoparticles based on multivalent peptide constructs. J. Am. Chem. Soc 2013, 135 (36), 13414–13424. [PubMed: 23978057]

(27). Murakami T Phospholipid nanodisc engineering for drug delivery systems. Biotechnol. J 2012, 7 (6), 762–767. [PubMed: 22581727]

(28). Ng KK; Lovell JF; Vedadi A; Hajian T; Zheng G Self-assembled porphyrin nanodiscs with structure-dependent activation for phototherapy and photodiagnostic applications. ACS Nano 2013, 7 (4), 3484–3490. [PubMed: 23464857]

(29). Sabnis N; Nair M; Israel M; McConathy WJ; Lacko AG Enhanced solubility and functionality of valrubicin (AD-32) against cancer cells upon encapsulation into biocompatible nanoparticles. Int. J. Nanomed 2012, 7, 975–983.

(30). Mooberry LK; Nair M; Paranjape S; McConathy WJ; Lacko AG Receptor mediated uptake of paclitaxel from a synthetic high density lipoprotein nanocarrier. J. Drug Target 2010, 18 (1), 53–58. [PubMed: 19637935]

(31). Duivenvoorden R; Tang J; Cormode DP; Mieszawska AJ; Izquierdo-Garcia D; Ozcan C; Otten MJ; Zaidi N; Lobatto ME; van Rijs SM; Priem B; Kuan EL; Martel C; Hewing B; Sager H; Nahrendorf M; Randolph GJ; Stroes ESG; Fuster V; Fisher EA; Fayad ZA; Mulder WJM A statin-loaded reconstituted high-density lipoprotein nanoparticle inhibits atherosclerotic plaque inflammation. Nat. Commun 2014, 5, 3065/1–12.

(32). Brouillette CG; Jones JL; Ng TC; Kercret H; Chung BH; Segrest JP Structural studies of apolipoprotein A-I/phosphatidylcholine recombinants by high-field proton NMR, nondenaturing gradient gel electrophoresis, and electron microscopy. Biochemistry 1984, 23 (2), 359–367. [PubMed: 6421314]

(33). Low H; Hoang A; Sviridov D Cholesterol efflux assay. J. Visualized Exp 2012, 61, No. e3810.

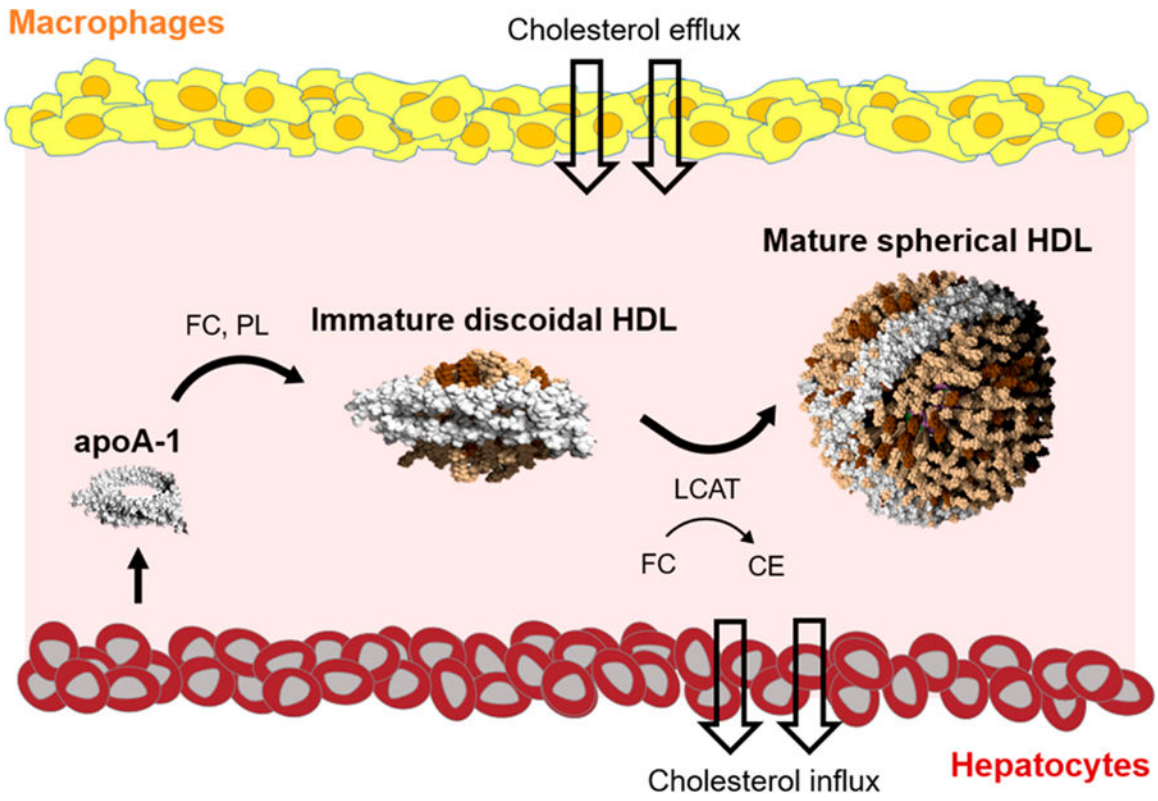

Figure 1.

Canonical reverse cholesterol transport pathway. Abbreviations: FC = free cholesterol, CE = cholesteryl esters, PL = phospholipids, and LCAT = lecithin:cholesterol acyltransferase.

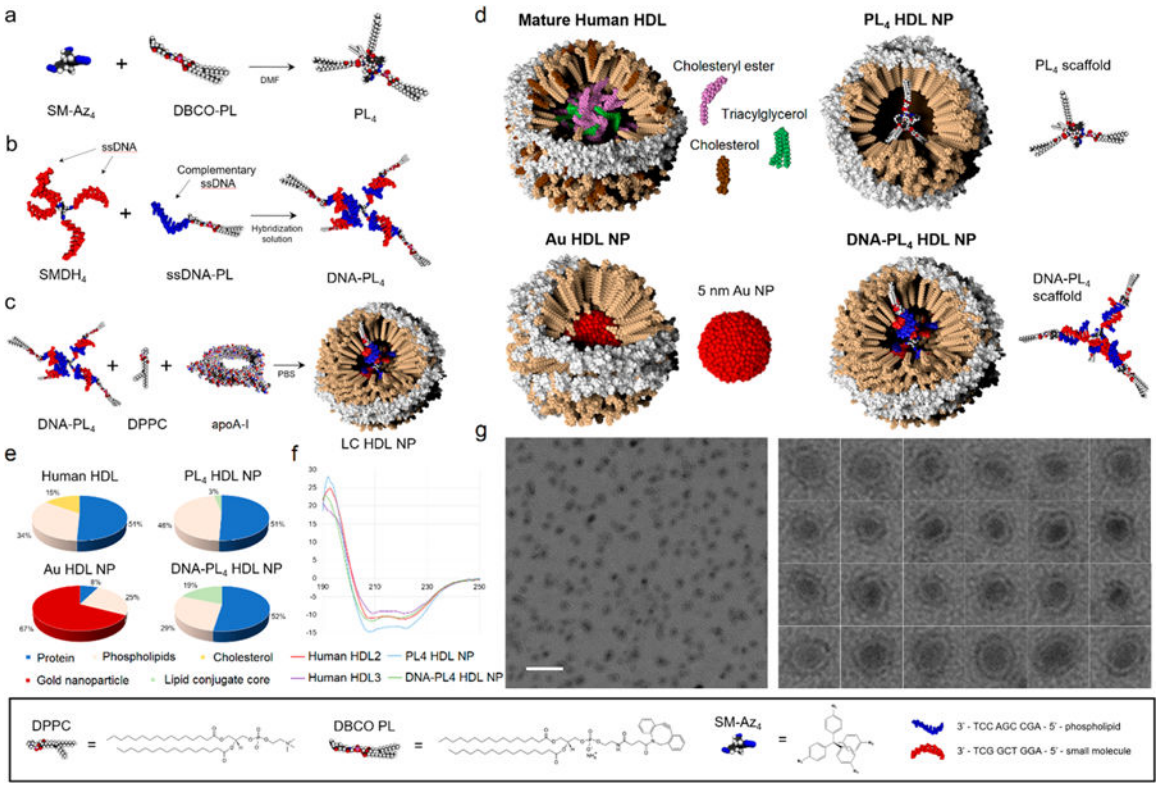

Figure 2.

(a–c) Synthesis schemes for PL_4 and DNA-PL_4 core scaffolds, and LC HDL NP assembly. (d) Schematic of native and synthetic HDLs. (e) Composition of native and synthetic HDLs by mass %. *Au HDL NP composition is reported from a previously published data set.[22] (f) Circular dichroism spectra for LC HDL NPs and human HDLs. (g) TEM imaging of DNA-PL_4 HDL NPs. Scale bar = 50 nm.

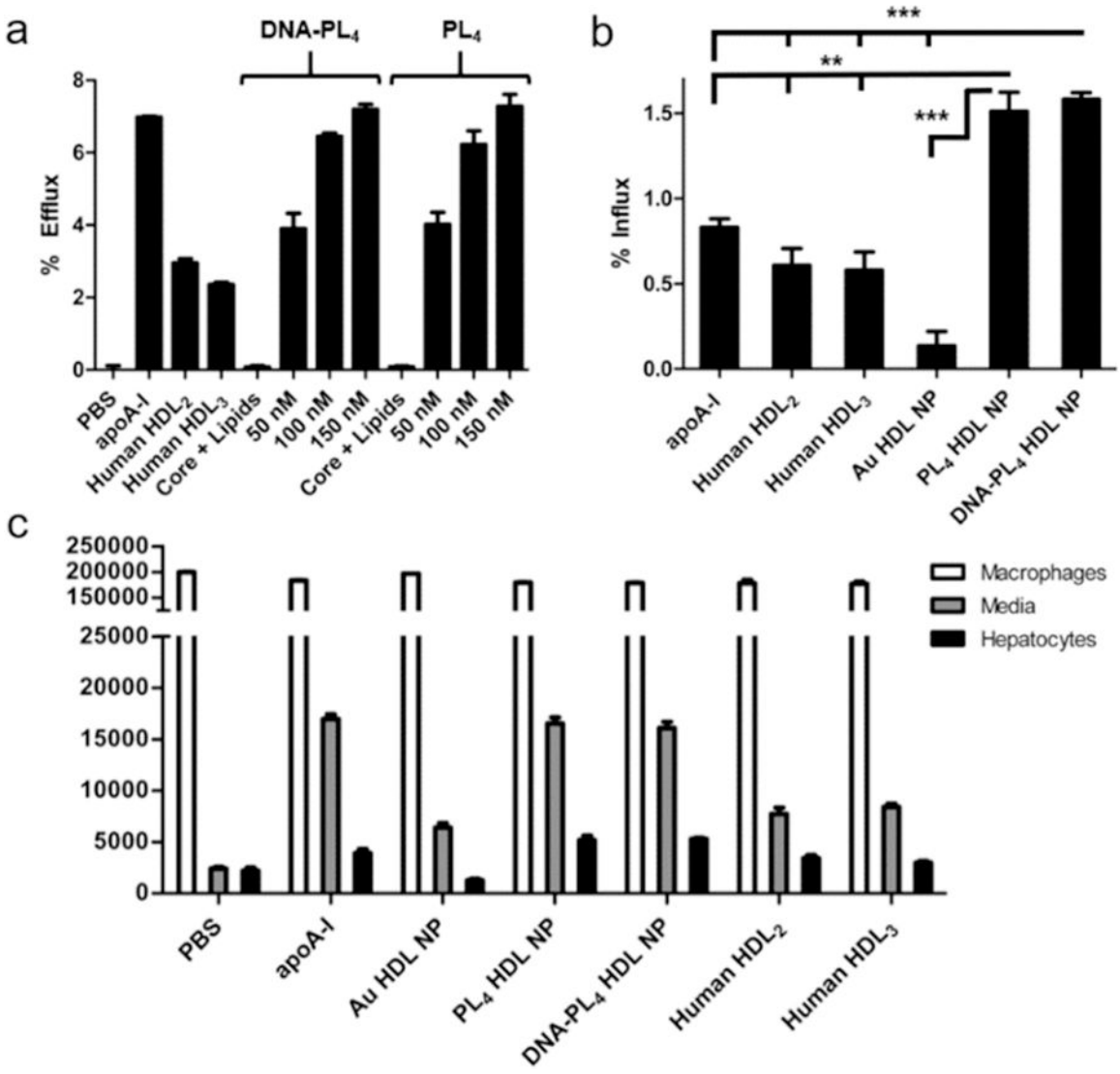

Figure 3.

(a) LC HDL NPs efflux [^{3}H]-chol from J774 macrophages. (b) % Influx of [^{3}H]-chol to HepG2 hepatocytes in a tandem efflux-influx assay. (c) Quantification of [^{3}H]-chol in all fractions from tandem assay. Two-tailed Student's *t* test: ** $p < 0.01$. *** $p < 0.001$.

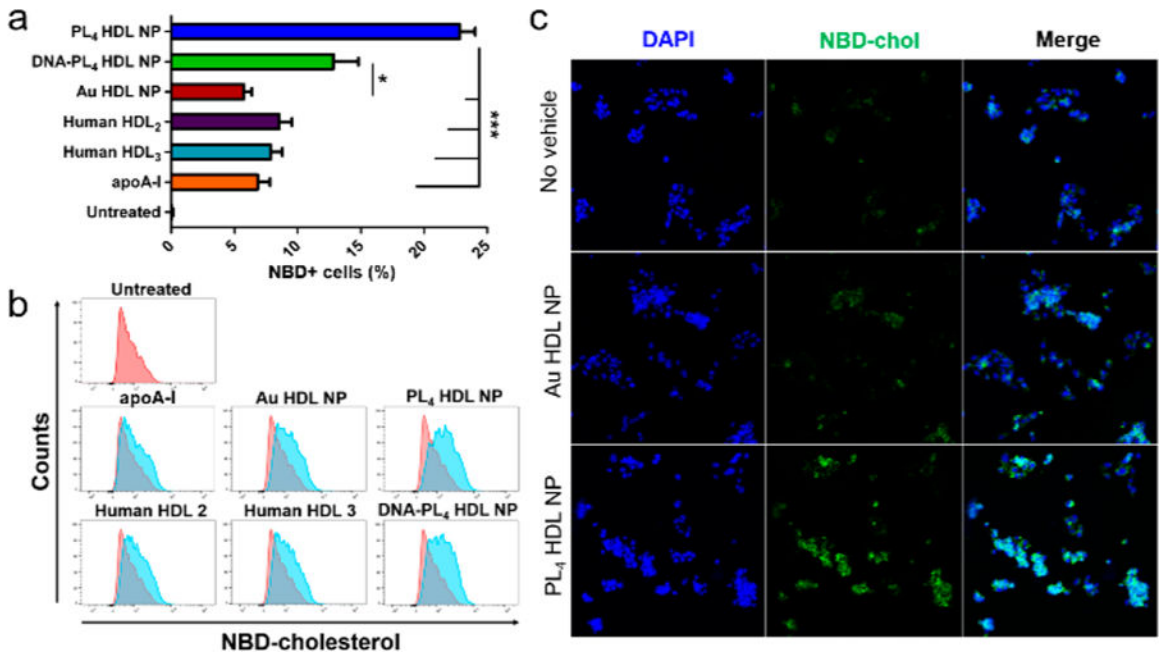

Figure 4.

LC HDL NPs facilitate delivery of NBD-chol to hepatocytes in 30 min via (a,b) flow cytometry and (c) confocal microscopy. Two-tailed Student's *t* test: $*p < 0.05$. $***p < 0.001$.

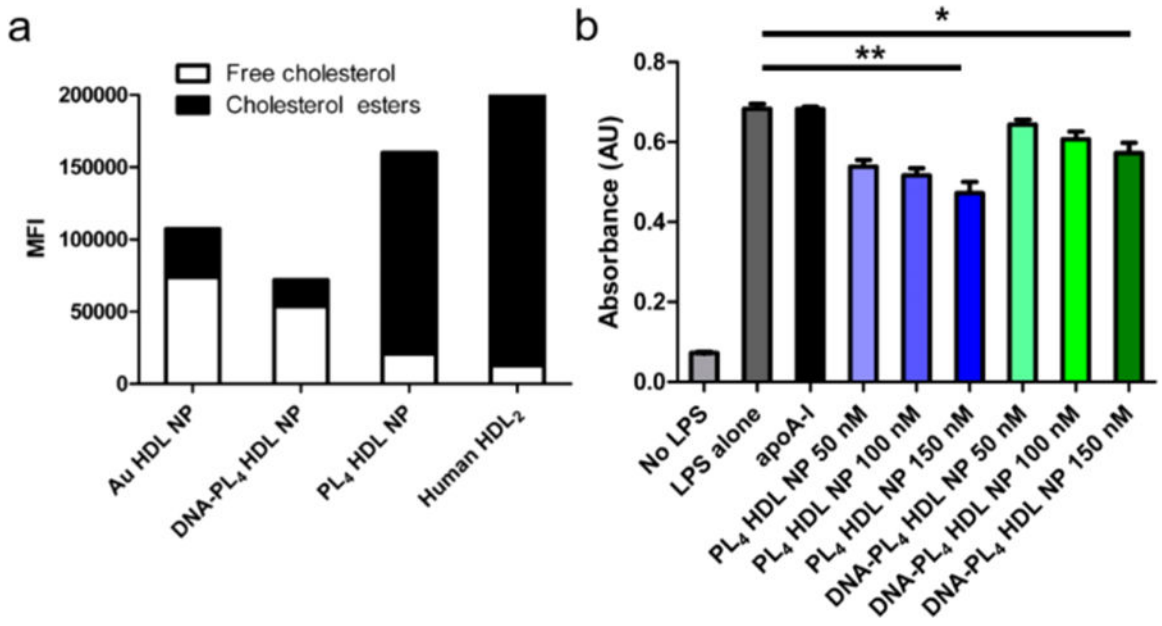

Figure 5.

(a) LC HDL NPs support LCAT-mediated cholesterol esterification. (b) LC HDL NPs suppress pro-inflammatory NF-κB signaling. Two-tailed Student's *t* test: *$p < 0.05$. ** $p < 0.01$.

Table 1.

Structural Analysis of Native and Synthetic HDLs via Circular Dichroism

	α-helix (%)	**β-sheet (%)**	**Turn (%)**	**Unordered (%)**
apoA-I	57 ± 3	4 ± 2	14 ± 3	25 ± 5
Au HDL NP	73 ± 1	0 ± 0	6 ± 1	21 ± 2
HDL_2	50 ± 2	7 ± 1	18 ± 4	24 ± 2
HDL_3	42 ± 1	15 ± 1	15 ± 1	28 ± 3
PL_4 HDL NP	50 ± 1	7 ± 1	16 ± 5	27 ± 1
DNA-PL_4 HDL NP	40 ± 1	20 ± 2	16 ± 2	25 ± 7